1. Effects of Neglecting Clinopyroxene or Plagioclase fractionation

The thermobarometric formulations in Lee et al. (2009) require knowledge regarding the primary magma composition, i.e., the composition of the magma when it was last in equilibrium with the mantle to calculate the average magma generation pressure (P_g) and temperature (T_g). As erupted magmas undergo some degree of mineral fractionation at crustal level, the primary magma composition has been inferred by reversing the fractionation process (Lee et al. 2009). Sometimes, the evolved magma is saturated with clinopyroxene and plagioclase along with olivine, and reversing the fractional crystallization of such magma is much difficult. This is because the exact proportion of each fractionating mineral is not known. To estimate the percentage of fractionation, the entire differentiation suite is necessary. To avoid this problem, Lee et al chose the most primitive magmas, similar to few previous workers (Putirka 2005; Herzberg et al. 2007; Herzberg and Asimow 2008, 2015), that have undergone olivine fractionation only. By negating plagioclase fractionation, the SiO_2 and MgO are overestimated. This results in somewhat higher T and P. Similarly, overlooking clinopyroxene fractionation underestimates SiO_2 and overestimates MgO, resulting in lower P and higher T.

2. Anhydrous source of origin for T_p calculation

Lee et al's thermobarometry can be applied for both hydrous and anhydrous magma. However, their formulations are calibrated to a minimum water content of 2 wt%, and considering lower water content than that suppresses the pressure estimation. Such high-water content magmas are characteristics of arc environment, where basalts generate through partial melting of a wet peridotite source. On the other hand, the ambient mantle derived basalts are originated from decompression melting of a dry peridotite source. Studies show that ambient mantle derived basalts (MORBs) contain a maximum up to 0.5 wt% of H_2O (Michael 1995; Sobolev and Chaussidon 1996; Danyushevsky 2001), and are dry magmas in nature. The T_p calculations from this study is based upon the ambient mantle derived basalts from Archean to Proterozoic. As discussed earlier, basalts derived from the ambient mantle are considered to be dry in nature. Therefore, all our calculations are conducted by assuming an anhydrous source of origin. Previous studies have also adopted a similar approach, considering an anhydrous source, to calculate the T_p of the ambient mantle (Komiya et al. 2002; Putirka 2005; Herzberg et al. 2010; Ganne and Feng 2017; Aulbach and Arndt 2019).

3. Assumptions regarding the final Mg# of olivine

To calculate P_g, and T_g, from the input basalts, Lee et al. (2009) applied a polybaric decompression melting model. Polybaric decompression melting initiated by solid-state upwelling, promotes melting along a path of changing pressure and temperature. The calculated primary melt composition in this process represents the weighted average aggregate melt composition. Lee et al. (2009) used a polybaric batch melting model to calculate the primary magma composition of a primitive basalt that has experienced only olivine fractionation. Batch melting refers to a process where the partial melt remains in equilibrium with its mantle residue at various melt fractions. Consequently, the authors have taken into account an average value of olivine Mg# to represent the mantle residuum. They first estimated an equilibrium olivine composition to the input basalt and added the olivine back into the magma until the magma equilibrates with olivine having an Mg# equivalent to the average mantle residuum. Varying the residuum Mg# to 1 unit can increase

or decrease the temperature upto 50-100°C.

We acknowledge that considering a final forsterite content might cause some uncertainties to our calculation. For example, the approach over-estimates temperatures if melting degrees are lower and under-estimates if melting degrees are higher. To reduce the inconsistency in assuming the final forsterite content, Herzberg and co-workers (Herzberg et al. 2007; Herzberg and Asimow 2008, 2015) simultaneously calculated the T_p and olivine Mg#. In other words, their approach is self-consistent and does not need a final olivine forsterite number to be fixed to calculate the T_p.

Note that the physical meaning of olivine Mg# in Herzberg's and Lee's methods differ. While the iteratively calculated olivine Mg# in Herzberg's method represents the Mg# of olivine to be crystallized from primary magma at 1 atmospheric pressure, the olivine Mg# required as input in Lee's method represents the Mg# of residual mantle source. This is because Herzberg's methodology to calculate primary magma composition is based on fractional melting equations, where the accumulated fractional melt is never in equilibrium with its residue except the final drop of liquid. Previous studies have shown that primary magmas produced by fractional melting have slightly higher FeO and lower SiO_2 content than batch melts at constant MgO content (Langmuir et al. 1992; Herzberg 2004). Later, Asimow and Longhi (2004) showed that primary melts, produced via accumulated fractional melting of fertile upper mantle peridotites can be very similar to that of batch melts in terms of MgO and FeO content.

Recent petrological estimations and studies of mantle-derived xenoliths suggest that the building blocks of the cratonic lithospheric mantle during the Archean and Proterozoic are residues left after basalt primary magma extraction in a typical hot-ridge setting, rather than from plume-related processes. For example, plume-related melting predominantly produces dunites, whereas most xenoliths from Archean and Proterozoic cratons are harzburgites, with very few dunitic populations. Further, the plume model predicts a gradual stratification from highly melt-depleted peridotite at shallow depths to fertile peridotites at the base, but such stratification is not a general feature of cratons (Lee et al. 2011). From mass balance calculations, Herzberg and Rudnick (2012) first calculated the nature of residue after melting in a hot-ridge setting. They found that the whole-rock Mg# of residues after basaltic primary magma extraction varies from 91.5-93.8 during the Archean and 91-92.7 during the Proterozoic (figure 4 in Herzberg and Rudnick (2012)). These values resemble the observed Mg# (whole-rock) as well as the olivine Mg# (Fo) in the cratonic lithospheric mantle. Based on this observation the authors suggested that the depleted peridotites from the Archean cratonic lithospheric mantle are the residual products of basaltic primary melt extraction in a typical hot mid-ocean ridge (MOR) setting rather than in a plume setting. These melt residues later became part of the continental lithospheric mantle through processes such as orogenesis or underthrusting. The basaltic crust was subsequently recycled to the mantle due to density inversion during subduction. Few of these Archean MOR basalts are preserved as non-arc basalts in Archean Greenstone belts. An *'Oceanic ridge origin of cratonic lithospheric mantle'* has been proposed by several other authors (Bickle 1986; Kelemen et al. 1998; Gibson et al. 2008; Herzberg et al. 2010; Rollinson 2010; Herzberg 2018; Servali and Korenaga 2018; Pearson et al. 2021).

Servali and Korenaga (2018) compiled mantle xenolith data from the continental lithosphere to constrain the secular evolution of mantle depletion since the Archean. By comparing the secular change in olivine Mg# from the Archean to the present with different present-day convecting Urey ratios ranging from 0.2-0.3, they concluded that the depleted peridotites in cratonic keels are the

residues of hot-ambient mantle melting during the Archean to Proterozoic and do not require an anomalously hotter plume source. They found that the olivine Mg# (Fo) (Mg/(Mg+Fe) × 100) varied from 90.5 to 93.5 during the Archean, with most olivine Mg# values distributed between 91.5 and 92.5 (their fig. 2b in the main text and supplementary fig. DR2). Pearson et al. (2021) made similar observations (their figure Box 2b). For Proterozoic the olivine Mg# varies from 89-93.

In terms of major oxide and REE concentrations, the Archean and Paleoproterozoic greenstone basalts presumably resembles compositionally with the Phanerozoic Ocean plateau basalts (e.g., Arndt et al. 2001; Condie 2005; Smithies et al. 2005). Herzberg and Gazel (2009) further demonstrated that the primary magma composition of the Ontong-Java Plateau basalts is similar to that of the primary magma composition of Archean and Paleoproterozoic non-arc basalts. This indicates that the Phanerozoic mantle plumes have similar temperatures to that of the Archean or Paleoproterozoic ambient mantle. Ishikawa et al. (2011) found an average olivine Mg# of 92 in the harzburgites from Malaita, south of the Ontong-Java Plateau, which are interpreted as the residual products of plume melting. However, the maximum T_p from Phanerozoic mantle plumes is restricted to ~ 1600 °C, whereas the maximum ambient mantle T_p during the Archean has been recorded as 1650 °C (Herzberg et al. 2010), indicating a higher residual olivine Mg# for some samples during the Archean.

T_p calculation in this study assumes a mean residual olivine Mg# (Mg/(Mg+Fe)) of 0.92 during the Archean and Proterozoic (fig. R1F1). However, a mean olivine Mg# of 0.92 might overestimate the potential temperature for Meso-Neoproterozoic samples and underestimate T_p for some Archean samples. Nonetheless, it would provide a range of T_p values from the Archean-Proterozoic, which can be compared with previous estimates to test the hot or cold Archean mantle hypothesis. For comparison, a residual olivine Mg# of 0.91 has been assumed to calculate T_p values during the Proterozoic, as presented in fig. R1F2.

Table R1T1 compares mantle potential temperature (T_p) values obtained through accumulated fractional melting and batch-melting model for non-arc basalts. The basalts were originally employed by Herzberg et al. (2010). The T_p values are re-calculated using their updated PRIMELT3 (Herzberg and Asimow 2015) algorithm and, concurrently, determined through the FRACTIONATE-PT software, incorporating an olivine Mg# of 0.92. Additionally, in both cases, the Fe^{+2}/Fe^{total} ratio was maintained at a constant value of 0.9.

Table R1T2 is similar to Table R1T1 except an olivine Fo value of 0.91 has been used for Proterozoic samples only to calculate the T_p^* (°C) and primary magma composition using FRACTIONATE-PT.

Table R1T1: Comparison between T_P values obtained from Archean to Proterozoic basalts using PRIMELT3 and FRACTIONATE-PT. The samples were originally used by Herzberg et al. (2010) **to calculate ambient mantle T_P using PRIMELT2 algorithm. The T_p^{AFM}(°C) is the mantle potential temperature obtained through Accumulated Fractional Melting (AFM) model using the updated PRIMELT program (PRIMELT3;** Herzberg and Asimow 2015**). T_p^* (°C) is calculated (see main text) using FRACTIONATE-PT** (Lee et al. 2009) **batch melting model by considering an average olivine residue of 0.92 in mantle. Assuming that the primary magma MgO content remains almost constant during decompression and the adiabatic path follows the MgO isopleth during decompression, $T_p^{PRIMELT3}$ (°C) has been estimated using the calculated primary magma MgO wt% from FRACTIONATE-PT, utilizing the formula $T_p^{PRIMELT3}$(°C) = 1025 + 28.6×MgO – 0.084×MgO^2. In all the cases a constant redox condition of Fe^{+2}/Fe^{total} = 0.9 has been assumed. The fields denoted by NA indicates that FRACTIONATE-PT is unable to calculate the primary magma composition from basalts having Σ total oxide elements < 97 wt%.**

Samples	Location	Age corrected (Ma)	T_p^{AFM}(°C)	T_p^* (°C)	$T_p^{PRIMELT3}$ (°C)	T_p^{AFM}- T_p^* (°C)	T_p^{AFM}- $T_p^{PRIMELT3}$ (°C)
gc010697	Coonterunah Gp, Pilbara	3520	1448.916	1455.662	1494.924	-6.745	-46.007
02MB256	Warrawoona	3450	1536.995	1566.212	1592.757	-29.217	-55.762
M-14-16	Minnesota, U.S.A.	3255	1624.858	1641.846	1657.824	-16.988	-32.966
96048540D	Sulfur Sprgs Gp, Pilbara	3246	1626.892				
485418	Ivisaartoq 1, Greenland	3075	1549.062	1575.902	1594.690	-26.840	-45.628
485420	Ivisaartoq 1, Greenland	3075	1514.470	1491.262	1524.943	23.207	-10.473
I-417	Iringora 'ophiolite' Finland	2800	1587.219	NA	NA	NA	NA
I-417/2	Iringora 'ophiolite' Finland	2800	1602.476	NA	NA	NA	NA
RKY-17	Kushtagi-Hungund, India	2746	1612.468	1560.290	1589.140	52.178	23.327
RKY-18	Kushtagi-Hungund, India	2746	1523.325	1535.926	1563.078	-12.600	-39.753
s MU96-20	Superior, Canada	2700	1488.887	1496.591	1526.143	-7.704	-37.256
s DH95-3	Superior, Canada	2700	1550.861	1557.537	1578.350	-6.675	-27.488
s T-7	Superior, Canada	2700	1545.850	1553.893	1586.391	-8.043	-40.541
2	Aravalli Supergroup, India	2550	1653.687	1648.235	1671.074	5.451	-17.387
9337	Lapland Basalts	2056	1516.610	NA	NA	NA	NA
CHK-MGO18	Cape Smith, Canada	1870	1604.981	1638.201	1653.792	-33.220	-48.811
CHK-MGO14	Cape Smith, Canada	1870	1534.580	1549.114	1575.765	-14.533	-41.184
CHK 215-8	Cape Smith, Canada	1870	1559.980	1605.946	1624.103	-45.966	-64.122
CHK 216-3	Cape Smith, Canada	1870	1534.878	1569.758	1591.271	-34.879	-56.393
CHK 217-5	Cape Smith, Canada	1870	1543.870	1576.296	1597.702	-32.426	-53.832
CHK 217-4	Cape Smith, Canada	1870	1558.443	1590.544	1607.893	-32.100	-49.450
CHK 220-2	Cape Smith, Canada	1870	1512.191	1514.734	1540.284	-2.543	-28.093
CHK 221-1	Cape Smith, Canada	1870	1505.827	1510.576	1535.096	-4.748	-29.268
CHK 221-3	Cape Smith, Canada	1870	1508.107	1512.034	1538.032	-3.927	-29.925

CHK 221-6	Cape Smith, Canada	1870	1534.572	1562.533	1586.481	-27.961	-51.908
CHK 221-7	Cape Smith, Canada	1870	1548.513	1576.300	1597.230	-27.786	-48.716
CHK 224-1	Cape Smith, Canada	1870	1557.138	1557.706	1576.845	-0.568	-19.706
27GV	Dubois, Colorado	1765	1495.725	1528.596	1552.095	-32.870	-56.369
18-4	Phulad 'ophiolite', India	1300	1495.659	1524.786	1553.086	-29.127	-57.426
05SC72-8	Rodinia, S China	800	1448.777	NA	NA	NA	NA
05SC72-8	Rodinia, S China	800	1425.348	NA	NA	NA	NA
05SC74-7	Rodinia, S China	800	1465.501	1479.064	1517.767	-13.563	-52.266

Table R1T2: Same as table R1T1 except shown only for Proterozoic basalts. T_p^* and primary magma composition for Proterozoic basalts has been estimated by assuming an olivine Fo value of 0.91.

Samples	Locations	Age Corrected (Ma)	T_p^{AFM}(°C)	T_p^* (°C)	$T_p^{PRIMELT3}$ (°C)	T_p^{AFM}- T_p^* (°C)	T_p^{AFM}- $T_p^{PRIMELT3}$ (°C)
9337	Lapland Basalts	2056	1516.611	NA	NA	NA	NA
CHK-MGO18	Cape Smith, Canada	1870	1604.981	1575.654	1591.121	29.327	13.860
CHK-MGO14	Cape Smith, Canada	1870	1534.580	1489.800	1516.722	44.781	17.859
CHK 215-8	Cape Smith, Canada	1870	1559.981	1547.467	1565.787	12.514	-5.807
CHK 216-3	Cape Smith, Canada	1870	1534.879	1511.937	1533.696	22.942	1.183
CHK 217-5	Cape Smith, Canada	1870	1543.870	1515.007	1536.741	28.863	7.129
CHK 217-4	Cape Smith, Canada	1870	1558.443	1530.342	1547.953	28.101	10.490
CHK 220-2	Cape Smith, Canada	1870	1512.191	1456.711	1482.196	55.480	29.995
CHK 221-1	Cape Smith, Canada	1870	1505.828	1456.460	1480.925	49.367	24.903
CHK 221-3	Cape Smith, Canada	1870	1508.107	1458.135	1484.063	49.972	24.044
CHK 221-6	Cape Smith, Canada	1870	1534.573	1504.245	1528.432	30.328	6.140
CHK 221-7	Cape Smith, Canada	1870	1548.513	1514.974	1536.203	33.539	12.310
CHK 224-1	Cape Smith, Canada	1870	1557.138	1498.451	1517.874	58.687	39.265
27GV	Dubois, Colorado	1765	1495.726	1475.836	1499.291	19.890	-3.565
18-4	Phulad 'ophiolite', India	1300	1495.660	1467.808	1496.093	27.851	-0.433
05SC72-8	Rodinia, S China	800	1448.777	NA	NA	NA	NA
05SC72-8	Rodinia, S China	800	1425.348	NA	NA	NA	NA
05SC74-7	Rodinia, S China	800	1465.501	1423.894	1462.139	41.607	3.362

Olivine Mg# ~ 0.92

For most of the samples during Archean, T_p^{AFM} is less than the apparent potential temperature (T_p^*) by 6 - 29 ℃ and less than $T_p^{PRIMELT3}$ by 17 - 55 ℃. In a few instances $T_p^{PRIMELT3}$ is less than T_p^{AFM} suggesting that the sample might be in equilibrium with a relatively more depleted olivine Mg# in the mantle. This observation, where T_p derived from the accumulated fractional melting model is lower than that from batch melts, is consistent with previous findings (Herzberg and Asimow 2015; Herzberg 2022). For Proterozoic basalts the T_p^{AFM} is less than T_p^* by 0.5 - 45 ℃, and less than $T_p^{PRIMELT3}$ by 19-64 ℃.

Olivine Mg# ~ 0.91

T_p^* is less than T_p^{AFM} for all Proterozoic basalts when calculated assuming a residual olivine Mg# of 0.91. Except for few samples during Paleo-Mesoproterozoic, $T_p^{PRIMELT3}$ from all other basalts is less than the T_p^{AFM}. Hence any T_p value observed during Proterozoic assuming an olivine Mg# of 0.91 might represent the minimum value.

Figure Captions

Fig. R1F1: Age vs. olivine Mg# from Archean to present (modified after Servali and Korenaga (2018); Pearson et al. (2021)). Olivine from Archean to Paleoproterozoic are mostly distributed between 91.5 to 92.5. The overall range of olivine Mg# during Archean ranges from 90.5-93.5, while during Proterozoic it ranges from 89-93.

Fig. R1F2: Variation in mantle potential temperature (T_p) with age. Orange circles represent T_p values calculated from basaltic magma generation temperature (T_g) and pressure (P_g) in the present study. An olivine Mg# of 0.92 has been considered for Archean basalts and 0.91 for Proterozoic basalts to calculate the primary magma composition, T_g and P_g. Redox conditions are considered as Fe^{+3}/Fe_{Total} = 0.1. The three Urey ratio values (0.08, 0.23, 0.38) are from Korenaga (2008). The black curve illustrates the thermal evolution of the MORB source mantle from Davies (2009) (D09), based on parameterized convection models with conventional heat-flow scaling. Ambient mantle T_p from non-arc basalts from Herzberg et al. (2010) are shown in yellow hexagons. Blue pentagons represent T_p solutions at redox conditions of Fe^{2+}/Fe_{Total} = 0.9 for non-arc basalts from Ganne and Feng (2017). Ambient mantle T_p variations from Ganne and Feng (2017) are shown with green curves: dashed (Fe^{2+}/Fe_{Total} = 0.8). The solid green curve represents the T_p variation calculated by Mitchell and Ganne (2022) at redox condition of Fe^{2+}/Fe_{Total} = 0.9, based on the analysis of Ganne and Feng (2017). T_p range for a pressure of 2.2 to 3.2 GPa based on the chemical composition of continental basalts e.g., condition in the arc mantle wedge from Keller and Schoene (2018) (K&S, 2018) are shown (shaded region). For comparison, T_p values from Komatiites and Phanerozoic Plume are shown (Herzberg 2022b). ML: Magmatic Lull from 2300 Ma to 2200 Ma (Spencer et al. 2018). Boring Billion from 1800 to 800 Ma (Roberts 2013).

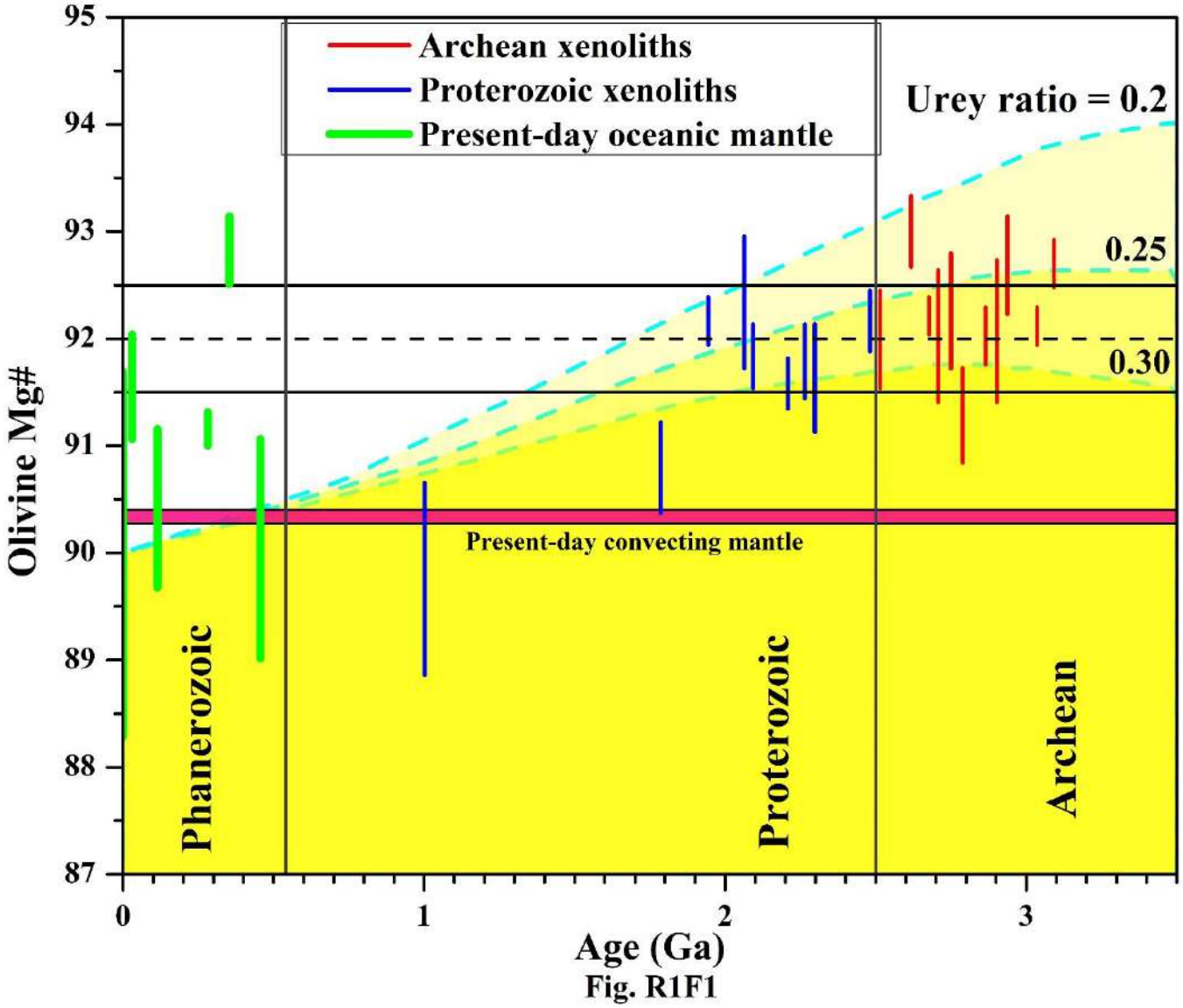
Archean xenoliths
Proterozoic xenoliths
Present-day oceanic mantle
Urey ratio = 0.2
0.25
0.30
Present-day convecting mantle
Phanerozoic
Proterozoic
Archean
Olivine Mg#
Age (Ga)
95
94
93
92
91
90
89
88
87
0
1
2
3

Fig. R1F1

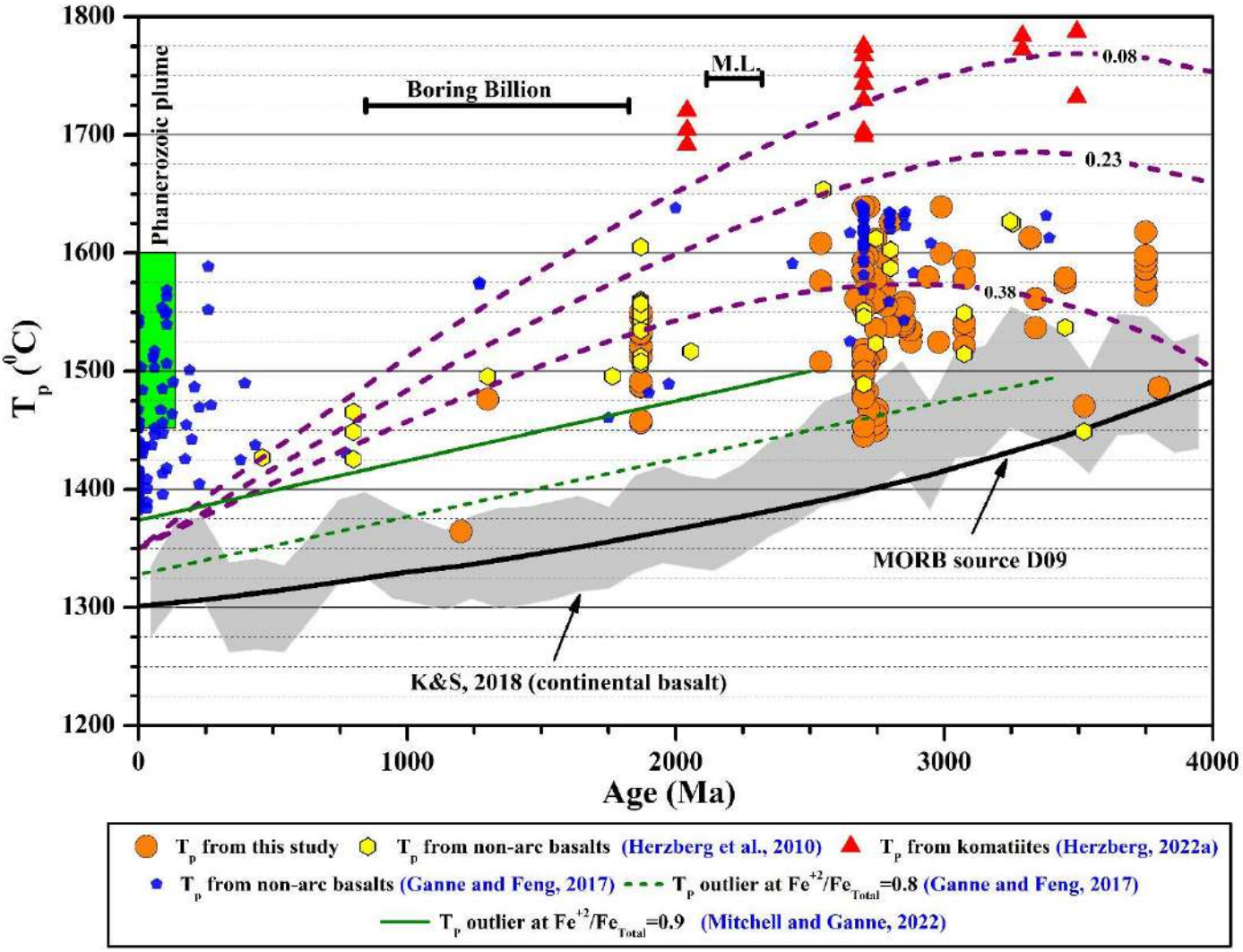
1800
1700
1600
1500
1400
1300
1200
T_p (^{0}C)
Phanerozoic plume
Boring Billion
M.L.
0.08
0.23
0.38
MORB source D09
K&S, 2018 (continental basalt)
0
1000
2000
3000
4000
Age (Ma)
T_p from this study
T_p from non-arc basalts (Herzberg et al., 2010)
T_p from komatiites (Herzberg, 2022a)
T_p from non-arc basalts (Ganne and Feng, 2017)
T_p outlier at Fe^{+2}/Fe_{Total}=0.8 (Ganne and Feng, 2017)
T_p outlier at Fe^{+2}/Fe_{Total}=0.9 (Mitchell and Ganne, 2022)

Fig. R1F2

References

Arndt N, Bruzak G, Reischmann T (2001) The oldest continental and oceanic plateaus: geochemistry of basalts and komatiites of the Pilbara Craton, Australia. Mantle plumes: their identification through time 359

Asimow PD, Longhi J (2004) The significance of multiple saturation points in the context of polybaric near-fractional melting. Journal of Petrology 45:2349–2367

Aulbach S, Arndt NT (2019) Eclogites as palaeodynamic archives: Evidence for warm (not hot) and depleted (but heterogeneous) Archaean ambient mantle. Earth Planet Sci Lett 505:162–172. https://doi.org/10.1016/j.epsl.2018.10.025

Bickle MJ (1986) Implications of melting for stabilisation of the lithosphere and heat loss in the Archaean. Earth Planet Sci Lett 80:314–324

Condie KC (2005) High field strength element ratios in Archean basalts: A window to evolving sources of mantle plumes? Lithos 79:491–504. https://doi.org/10.1016/j.lithos.2004.09.014

Danyushevsky L V (2001) The effect of small amounts of H2O on crystallisation of mid-ocean ridge and backarc basin magmas. Journal of Volcanology and Geothermal Research 110:265–280

Davies GF (2009) Effect of plate bending on the Urey ratio and the thermal evolution of the mantle. Earth Planet Sci Lett 287:513–518. https://doi.org/10.1016/j.epsl.2009.08.038

Ganne J, Feng X (2017) Primary magmas and mantle temperatures through time. Geochemistry, Geophysics, Geosystems 18:872–888. https://doi.org/10.1002/2016GC006787.Received

Gibson SA, Malarkey J, Day JA (2008) Melt depletion and enrichment beneath the western Kaapvaal Craton: evidence from Finsch peridotite xenoliths. Journal of Petrology 49:1817–1852

Herzberg C (2004) Geodynamic information in peridotite petrology. Journal of Petrology 45:2507–2530. https://doi.org/10.1093/petrology/egh039

Herzberg C (2018) From hot oceanic ridges to cool cratons. Geology 46:1079–1080

Herzberg C (2022) Understanding the Paleoproterozoic Circum-Superior Large Igneous Province constrains the thermal properties of Earth's mantle through time. Precambrian Res 375:. https://doi.org/10.1016/j.precamres.2022.106671

Herzberg C, Asimow PD (2015) PRIMELT3 MEGA.XLSM software for primary magma calculation: Peridotite primary magma MgO contents from the liquidus to the solidus. Geochemistry, Geophysics, Geosystems 16:563–578. https://doi.org/10.1002/2014GC005631.

Herzberg C, Asimow PD (2008) Petrology of some oceanic island basalts: PRIMELT2.XLS software for primary magma calculation. Geochemistry, Geophysics, Geosystems 9:. https://doi.org/10.1029/2008GC002057

Herzberg C, Asimow PD, Arndt N, et al (2007) Temperatures in ambient mantle and plumes: Constraints from basalts, picrites, and komatiites. Geochemistry, Geophysics, Geosystems 8:. https://doi.org/10.1029/2006GC001390

Herzberg C, Condie K, Korenaga J (2010) Thermal history of the Earth and its petrological expression. Earth Planet Sci Lett 292:79–88. https://doi.org/10.1016/j.epsl.2010.01.022

Herzberg C, Gazel E (2009) Petrological evidence for secular cooling in mantle plumes. Nature 458:619–622

Herzberg C, Rudnick R (2012) Formation of cratonic lithosphere: An integrated thermal and petrological model. Lithos 149:4–15. https://doi.org/10.1016/j.lithos.2012.01.010

Ishikawa A, Pearson DG, Dale CW (2011) Ancient Os isotope signatures from the Ontong Java Plateau lithosphere: Tracing lithospheric accretion history. Earth Planet Sci Lett 301:159–170

Kelemen PB, Hart SR, Bernstein S (1998) Silica enrichment in the continental upper mantle via melt/rock reaction. Earth Planet Sci Lett 164:387–406

Keller B, Schoene B (2018) Plate tectonics and continental basaltic geochemistry throughout Earth history. Earth Planet Sci Lett 481:290–304

Komiya T, Maruyama S, Hirata T, Yurimoto H (2002) Petrology and Geochemistry of MORB and OIB in the Mid-Archean North Pole Region, Pilbara Craton, Western Australia: Implications for the Composition and Temperature of the Upper Mantle at 3.5 Ga. Int Geol Rev 44:988–1016. https://doi.org/10.2747/0020-6814.44.11.988

Korenaga J (2008) Urey ratio and the structure and evolution of Earth's mantle. Reviews of Geophysics 46:1–32. https://doi.org/10.1029/2007RG000241

Langmuir CH, Klein EM, Plank T (1992) Petrological systematics of mid-ocean ridge basalts: Constraints on melt generation beneath ocean ridges. Mantle flow and melt generation at mid-ocean ridges 71:183–280

Lee C-TA, Luffi P, Chin EJ (2011) Building and destroying continental mantle. Annu Rev Earth Planet Sci 39:59–90

Lee C-TA, Luffi P, Plank T, et al (2009) Constraints on the depths and temperatures of basaltic magma generation on Earth and other terrestrial planets using new thermobarometers for mafic magmas. Earth Planet Sci Lett 279:20–33

Michael P (1995) Regionally distinctive sources of depleted MORB: Evidence from trace elements and H2O. Earth Planet Sci Lett 131:301–320

Mitchell RN, Ganne J (2022) Less is not always more: A more inclusive data-filtering approach to secular mantle cooling. Precambrian Res 379:106787

Pearson DG, Scott JM, Liu J, et al (2021) Deep continental roots and cratons. Nature 596:199–210

Putirka KD (2005) Mantle potential temperatures at Hawaii, Iceland, and the mid-ocean ridge system, as inferred from olivine phenocrysts: Evidence for thermally driven mantle plumes. Geochemistry, Geophysics, Geosystems 6:

Roberts NMW (2013) The boring billion?–Lid tectonics, continental growth and environmental change associated with the Columbia supercontinent. Geoscience Frontiers 4:681–691

Rollinson H (2010) Coupled evolution of Archean continental crust and subcontinental lithospheric mantle. Geology 38:1083–1086

Servali A, Korenaga J (2018) Oceanic origin of continental mantle lithosphere. Geology 46:1047–1050

Smithies RH, Van Kranendonk MJ, Champion DC (2005) It started with a plume–early Archaean basaltic proto-continental crust. Earth Planet Sci Lett 238:284–297

Sobolev A V, Chaussidon M (1996) H2O concentrations in primary melts from supra-subduction zones and mid-ocean ridges: implications for H2O storage and recycling in the mantle. Earth Planet Sci Lett 137:45–55

Spencer CJ, Murphy JB, Kirkland CL, et al (2018) A Palaeoproterozoic tectono-magmatic lull as a potential trigger for the supercontinent cycle. Nat Geosci 11:97–101. https://doi.org/10.1038/s41561-017-0051-y